

Aerodynamic stability analysis of geometrically nonlinear orthotropic membrane structure with hyperbolic paraboloid in sag direction

Yun-ping Xu^{*1}, Zhou-lian Zheng², Chang-jiang Liu³, Kui Wu⁴ and Wei-ju Song⁴

¹China Resources Land Limited (Chongqing), Chongqing 400050, P.R. China

²College of Civil Engineering, Chongqing Univ., Chongqing 400045, P. R. China; and Chongqing JUANZHU College, Chongqing 400072, P.R. China

³State Key Laboratory of Geohazard Prevention and Geoenvironment Protection, Chengdu University of Technology, Chengdu, 610059, China

⁴College of Civil Engineering, Chongqing Univ., Chongqing 400045, P.R. China

(Received March 2, 2017, Revised February 6, 2018, Accepted February 8, 2018)

Abstract. This paper studies the aerodynamic stability of a tensioned, geometrically nonlinear orthotropic membrane structure with hyperbolic paraboloid in sag direction. Considering flow separation, the wind field around membrane structure is simulated as the superposition of a uniform flow and a continuous vortex layer. By the potential flow theory in fluid mechanics and the thin airfoil theory in aerodynamics, aerodynamic pressure acting on membrane surface can be determined. And based on the large amplitude theory of membrane and D'Alembert's principle, interaction governing equations of wind-structure are established. Then, under the circumstance of single-mode response, the Bubnov-Galerkin approximate method is applied to transform the complicated interaction governing equations into a system of second-order nonlinear differential equation with constant coefficients. Through judging the frequency characteristic of the system characteristic equation, the critical velocity of divergence instability is determined. Different parameter analysis shows that the orthotropy, geometrical nonlinearity and scantling of structure is significant for preventing destructive aerodynamic instability in membrane structures. Compared to the model without considering flow separation, it's basically consistent about the divergence instability regularities in the flow separation model.

Keywords: membrane structure; orthotropy; geometrical nonlinearity; flow separation; aerodynamic instability; critical velocity of divergence instability

1. Introduction

Because of its economy, beauty and low deadweight, membrane structure is widely applied to long-span structures such as stadiums, exhibition centers and works of decoration. But for its low deadweight, low local stiffness and low natural frequency, this kind of structure is very sensitive to wind load. We can't ignore the interaction between membrane structures and wind environment, and it can be evaluated by two parameters, added mass and radiation /aerodynamic damping through experimentally investigating (Minami 1998, Yang *et al.* 2010, Liu *et al.* 2016). In order to investigate the general trend of the aerodynamic behavior, Rizzo (2015, 2016) adopt static loads to simulate dynamic effects of wind on hyperbolic paraboloid roofs with square plan, through wind tunnel tests and CFD analyses, and explore the possibility of defining equivalent static pressure fields able to reproduce the envelope of dynamic displacements of the cables net.

As the wind velocity reaches a certain value, aerodynamic instability phenomena may occur. In wind-tunnel tests for suspended cable roof models, Miyake *et al.* (1992) and Kawakita *et al.* (1992) observed this kind of

aerodynamic instability phenomenon. In actual engineering, the membrane roofs of the Cheju World Cup stadium in Korea and Wenzhou University stadium in China have experienced local destruction under the wind loads of less than design value. It has caused scholars to pay attention to the aerodynamic stability of membrane structure under wind loads. At present, there has been an agreement of qualitative analysis about the mechanism of aerodynamic instability in tensioned membrane structure (Minami *et al.* 1993, Sun *et al.* 2003, Yang *et al.* 2005). These studies found that at a lower wind velocity, the structure vibrates primarily in single-mode for divergence instability. With the velocity increasing, it presents a vibrating trend of multimode coupling for flutter instability. However, studies on quantitative analysis are poor. Sygulski (1994, 1997) applied FEM (finite element modeling) and BEM (boundary element method) to deduce the critical velocity of instability with a membrane model supported on a rigid board in the uniform potential flow. Attar *et al.* (2005), Munteanu *et al.* (2015) used a reduced-order system-identifying approach to analyze the structural nonlinear behavior of aeroelastic configurations, and the results matched well with those from a high-fidelity aeroelastic model, in a similar way Vassilopoulou *et al.* (2012) studied the nonlinear dynamic phenomena in a SDOF model of cable net, and the numerical analyses approaches well the behavior of analytical solutions of the simplified model.

*Corresponding author
E-mail: david_hsu9@163.com

With the small deformation theory, Banichuk *et al.* (2010a, b) analyzed the stability of membranes and plates interacting with axially moving ideal fluid, and obtained the critical velocity of divergence instability by numerical method. Stanford *et al.* (2007, 2008) invented a novel experimental facility that integrated wind tunnel with a visual image-correlation system for simultaneous measurement of wing displacements, strains and aerodynamic loads, and the numerical and experimental data have suitable correspondence for moderate angles of attack. Combined with a finite-difference membrane model with third-order piston theories, Scott *et al.* (2007) used Nastran normal modes in the structured compressible flow solver to simulate the dynamic aeroelastic stability of membrane structures for aerocapture, and the results obtained are consistent with a static aeroelastic analysis. Yang *et al.* (2006) used an analytic method to derive the critical instability wind velocity of a tensioned membrane model by judging the stability of the wind-roof interaction equation. Li *et al.* (2006) did this by judging the frequency characteristic of the system characteristic equation. By large amplitude theory and the D'Alembert's principle and taking structure's geometric nonlinearity and orthotropy in consideration, Zheng *et al.* (2010) and Xu *et al.* (2011) summarized Yang and Li's research thinking, and obtained the critical velocities of divergence instability of membrane model with planar and hyperbolic paraboloid in arch direction under the ideal potential flow.

This paper presents a theoretical study of the aerodynamic stability of a tensioned membrane model with hyperbolic paraboloid in sag direction, including the tow characteristics of orthotropy and geometric nonlinearity in actual engineering. On the basis of large amplitude theory and D'Alembert's principle, the governing equation is addressed in the subsequent section. Applying the Bubnov-Galerkin approximate method, the next section is devoted to deducing the critical velocity of divergence instability. Referring to the analysis with the model in arch direction (Xu *et al.* 2011), computational examples are given to analyze the aerodynamic instability rules affected by each parameter. Some conclusions are also presented.

2. Governing equation

2.1 Structure model and boundary conditions

The hyperbolic paraboloid membrane model studied is orthotropic, with differential Young's moduli in its two principal fiber directions. Assume that the two principal fiber directions are just along with the two orthogonal directions x and y in a three-dimensional (3D) Cartesian coordinate system; see Fig. 1. The four edges of the model are completely clamped immovably. The spans in x and y are denoted by a and b , respectively; the initial stress in x and y are denoted by N_{0x} and N_{0y} , respectively. The membrane's center point O' is in the plane xoy . The wind direction is along the structure's sag direction, namely y direction.

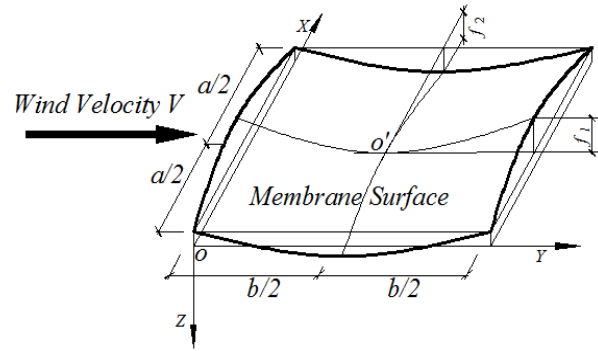


Fig. 1 Tensioned orthotropic hyperbolic paraboloid membrane model with four edges clamped (wind along y direction)

The initial surface function is

$$z_0(x, y) = \frac{f_2 \left(x - \frac{a}{2}\right)^2}{\left(\frac{a}{2}\right)^2} - \frac{f_1 \left(y - \frac{b}{2}\right)^2}{\left(\frac{b}{2}\right)^2} \quad (1)$$

where f_1 denotes the midspan sag in y , and f_2 denotes the midspan arch in x .

The initial principal curvatures in x and y are

$$\begin{cases} k_{0x} = \frac{\partial^2 z_0}{\partial x^2} = \frac{8f_2}{a^2} \\ k_{0y} = \frac{\partial^2 z_0}{\partial y^2} = \frac{-8f_1}{b^2} \end{cases} \quad (2)$$

Under the action of N_{0x} and N_{0y} , the equilibrium equation is obtained

$$N_{0x}k_{0x} + N_{0y}k_{0y} = 0 \quad (3)$$

Let

$$\gamma = N_{0y} / N_{0x}, \quad \lambda = a / b, \quad \varepsilon = f_1 / b$$

The displacement boundary conditions can be expressed as follows

$$\begin{cases} w(0, y, t) = 0 \\ w(a, y, t) = 0 \end{cases} \quad \begin{cases} w(x, 0, t) = 0 \\ w(x, b, t) = 0 \end{cases} \quad (4)$$

where w =denotes deflection: $w(x, y, t)$.

2.2 Dynamic governing equations

According to the large amplitude theory and D'Alembert's principle, the dynamic equilibrium equation and the compatible equation of orthotropic membrane are (Liu *et al.* 2013, Awrejcewicz 2013)

$$\begin{cases} k_{0x}h\frac{\partial^2\varphi}{\partial y^2}+k_{0y}h\frac{\partial^2\varphi}{\partial x^2}+\left(h\frac{\partial^2\varphi}{\partial y^2}+N_{0x}\right)\frac{\partial^2 w}{\partial x^2}+\left(h\frac{\partial^2\varphi}{\partial x^2}+N_{0y}\right)\frac{\partial^2 w}{\partial y^2}-2\rho_0\xi_0\frac{\partial w}{\partial t}+p_2-p_1=\rho_0\frac{\partial^2 w}{\partial t^2} \\ \frac{1}{E_1}\frac{\partial^4\varphi}{\partial y^4}+\frac{1}{E_2}\frac{\partial^4\varphi}{\partial x^4}=\left(\frac{\partial^2 w}{\partial x\partial y}\right)^2-\frac{\partial^2 w}{\partial x^2}\frac{\partial^2 w}{\partial y^2}-\left(k_{0x}\frac{\partial^2 w}{\partial y^2}+k_{0y}\frac{\partial^2 w}{\partial x^2}\right) \end{cases} \quad (5)$$

where h = membrane's thickness; ρ_0 = membrane's area density; ξ_0 = structure's self-damping coefficient; p_1 and p_2 = atmospheric pressure of lower and upper surface, respectively (p_1 = static atmospheric pressure p_∞); E_1 and E_2 = Young's moduli in x and y , respectively; φ = stress function: $\varphi(x, y, t)$.

3 Critical velocity of divergence instability

3.1 Aerodynamics

Dowell (1970) and Tang (2015) pointed out the air viscosity should be considered if the vibration wavelength is close to the air boundary layer thickness. But in civil engineering structures, the low-order mode often plays a dominant role when vibrating, so the wavelength is far greater than the boundary layer thickness. The experimental studies of Uematsu *et al.* (2009) showed that the boundary-layer turbulence has little effect on the structural response under wind loads. In this paper, the potential flow is considered to be inviscid, uniform and incompressible. Assume the flow is over the upper surface of the structure only, flow velocity V and direction along y , namely the sag direction of the structure; see Fig. 1. Due to the sharp corner of the structure's leading edge, it would present a flow separation phenomenon and a vortex disturbance layer when flow encounters the structure. In this case, the disturbance layer can be simulated in a razor-thin & continuous vortex layer approximately. So the wind field above the structure can be simulated in superposition of a uniform flow and a continuous vortex layer.

According to the fluid Bernoulli's equation, the outdoor pressure p_2 is (Forsching 1980)

$$p_2 = -\rho\left(V\frac{\partial\phi'}{\partial y} + \frac{\partial\phi'}{\partial t}\right) + p_\infty \quad (6)$$

where ρ = air density; ϕ' = velocity perturbation potential: $\phi'(x, y, z, t)$; p_∞ = static atmospheric pressure; V = flow velocity.

According to the potential theory, $\phi'(x, y, z, t)$ in Eq. (6) needs to satisfy Laplace's equation [Eq. (7)] and boundary condition [Eq. (8)]

$$\frac{\partial^2\phi'}{\partial x^2} + \frac{\partial^2\phi'}{\partial y^2} + \frac{\partial^2\phi'}{\partial z^2} = 0 \quad (7)$$

$$v_z = \frac{\partial\phi'}{\partial z} = V\frac{\partial z}{\partial x} + \frac{\partial z}{\partial t} \quad (8)$$

where v_z = flow velocity component in z .

According to the thin airfoil theory in aerodynamics, $\phi'(x, y, z, t)$ satisfying Eqs. (7) and (8) can be supposed as follows (Ivovich *et al.* 1991, Yang *et al.* 2006)

$$\phi'(x, y, t) = -\int_0^y \gamma(x, \eta, t) d\eta \quad (9)$$

where γ = the vortex density: $\gamma(x, y, t)$.

Substituting Eq. (9) into Eq. (6) yields

$$p_2 = \rho V \gamma + \rho \int_0^y \frac{\partial\gamma(x, \eta, t)}{\partial t} d\eta + p_\infty \quad (10)$$

3.2 Critical velocity of divergence instability

Substituting Eq. (10) into Eq. (5) yields

$$\begin{aligned} k_{0x}h\frac{\partial^2\varphi}{\partial y^2}+k_{0y}h\frac{\partial^2\varphi}{\partial x^2}+\left(h\frac{\partial^2\varphi}{\partial y^2}+N_{0x}\right)\frac{\partial^2 w}{\partial x^2}+\left(h\frac{\partial^2\varphi}{\partial x^2}+N_{0y}\right)\frac{\partial^2 w}{\partial y^2} \\ -2\rho_0\xi_0\frac{\partial w}{\partial t} + \rho V \gamma + \rho \int_0^y \frac{\partial\gamma}{\partial t} d\eta = \rho_0\frac{\partial^2 w}{\partial t^2} \end{aligned} \quad (11)$$

According to the Bubnov-Galerkin method, functions that satisfy the boundary conditions Eq. (4) are as follows

$$\begin{cases} w(x, y, t) = \sum_{i=1}^n T_i(t) W_i(x, y) \\ \varphi(x, y, t) = \sum_{i=1}^n T_i(t) \Phi_i(x, y) \end{cases} \quad (12)$$

where $W_i(x, y)$ = mode shape function; $\Phi_i(x, y)$ = coordinate stress function; $T_i(t)$ and $\tilde{T}_i(t)$ = time functions.

These studies (Minami *et al.* 1993, Sun *et al.* 2003, Yang *et al.* 2005) found that at a lower wind velocity, the structure vibrates primarily in single-mode for divergence instability, with the velocity increasing, it presents a vibrating trend of multimode coupling for flutter instability. As the flutter instability is a multimode coupling instability, and it is difficult to solve this kind of nonlinear equation. This paper studies the divergence instability on the basis of single-mode structural vibration.

Assume the single-mode shape function that satisfies the boundary conditions Eq. (4) is

$$W(x, y) = \sin\frac{m\pi x}{a} \sin\frac{n\pi y}{b} \quad (13)$$

where m and n = orders of vibration mode in x and y , respectively.

So the displacement function is

$$w(x, y, t) = T(t) \sin\frac{m\pi x}{a} \sin\frac{n\pi y}{b} \quad (14)$$

Substituting Eq. (14) into Eq. (5) yields

$$\frac{1}{E_1} \frac{\partial^4 \varphi}{\partial y^4} + \frac{1}{E_2} \frac{\partial^4 \varphi}{\partial x^4} = \frac{m^2 n^2 \pi^4}{2a^2 b^2} T^2(t) \left(\cos \frac{2m\pi x}{a} + \cos \frac{2n\pi y}{b} \right) + \left(k_{0x} \frac{n^2 \pi^2}{b^2} + k_{0y} \frac{m^2 \pi^2}{a^2} \right) T(t) \sin \frac{m\pi x}{a} \sin \frac{n\pi y}{b} \quad (15)$$

Assume that the stress function which satisfied Eq. (15) is

$$\begin{cases} \varphi(x, y, t) = T^2(t)\Phi_1(x, y) + T(t)\Phi_2(x, y) \\ \Phi_1(x, y) = \left(\alpha \cos \frac{2m\pi x}{a} + \beta \cos \frac{2n\pi y}{b} \right) \\ \Phi_2(x, y) = \delta \sin \frac{m\pi x}{a} \sin \frac{n\pi y}{b} = \delta W(x, y) \end{cases} \quad (16)$$

Substituting Eq. (16) into Eq. (15) yields

$$\begin{cases} \alpha = \frac{E_2 a^2 n^2}{32 b^2 m^2} \\ \beta = \frac{E_1 b^2 m^2}{32 a^2 n^2} \\ \delta = \frac{k_{0x} (n\pi/b)^2 + k_{0y} (m\pi/a)^2}{(n\pi/b)^4 / E_1 + (m\pi/a)^4 / E_2} \end{cases} \quad (17)$$

Substituting Eqs. (14) and (16) into Eq. (11) yields

$$\begin{aligned} & \rho_0 W T''(t) + 2\rho_0 \xi_0 W T'(t) - \left(k_{0x} h \frac{\partial^2 \Phi_2}{\partial y^2} + k_{0y} h \frac{\partial^2 \Phi_2}{\partial x^2} + N_{0x} \frac{\partial^2 W}{\partial x^2} + N_{0y} \frac{\partial^2 W}{\partial y^2} \right) T(t) \\ & - h \left(k_{0x} \frac{\partial^2 \Phi_1}{\partial y^2} + k_{0y} \frac{\partial^2 \Phi_1}{\partial x^2} + \frac{\partial^2 \Phi_2}{\partial y^2} \frac{\partial^2 W}{\partial x^2} + \frac{\partial^2 \Phi_2}{\partial x^2} \frac{\partial^2 W}{\partial y^2} \right) T^2(t) \\ & - h \left(\frac{\partial^2 \Phi_1}{\partial y^2} \frac{\partial^2 W}{\partial x^2} + \frac{\partial^2 \Phi_1}{\partial x^2} \frac{\partial^2 W}{\partial y^2} \right) T^3(t) - \rho V \gamma - \rho \int_0^y \frac{\partial \gamma}{\partial t} d\eta = 0 \end{aligned} \quad (18)$$

According to the Bubnov-Galerkin method (Shin *et al.* 2004), Eq. (18) can be transformed as follows

$$\iint_S \left\{ \begin{aligned} & \rho_0 W T''(t) + 2\rho_0 \xi_0 W T'(t) \\ & - \left(k_{0x} h \frac{\partial^2 \Phi_2}{\partial y^2} + k_{0y} h \frac{\partial^2 \Phi_2}{\partial x^2} + N_{0x} \frac{\partial^2 W}{\partial x^2} + N_{0y} \frac{\partial^2 W}{\partial y^2} \right) T(t) \\ & - h \left(k_{0x} \frac{\partial^2 \Phi_1}{\partial y^2} + k_{0y} \frac{\partial^2 \Phi_1}{\partial x^2} + \frac{\partial^2 \Phi_2}{\partial y^2} \frac{\partial^2 W}{\partial x^2} + \frac{\partial^2 \Phi_2}{\partial x^2} \frac{\partial^2 W}{\partial y^2} \right) T^2(t) \\ & - h \left(\frac{\partial^2 \Phi_1}{\partial y^2} \frac{\partial^2 W}{\partial x^2} + \frac{\partial^2 \Phi_1}{\partial x^2} \frac{\partial^2 W}{\partial y^2} \right) T^3(t) - \rho V \gamma - \rho \int_0^y \frac{\partial \gamma}{\partial t} d\eta \end{aligned} \right\} W(x, y) dx dy = 0 \quad (19)$$

where $S \in \{0 \leq x \leq a, 0 \leq y \leq b\}$.

Eq. (19) can be simplified as

$$AT''(t) + BT'(t) - CT(t) - DT^2(t) - ET^3(t) - F = 0 \quad (20)$$

where

$$\begin{aligned} A &= \iint_S \rho_0 W^2 dx dy = \frac{\rho_0 ab}{4} \\ B &= 2\rho_0 \xi_0 \iint_S W^2 dx dy \\ &= 2\rho_0 \xi_0 \iint_S \left(\sin \frac{m\pi x}{a} \sin \frac{n\pi y}{b} \right)^2 dx dy \\ &= \frac{\rho_0 \xi_0 ab}{2} \end{aligned}$$

$$\begin{aligned} C &= \iint_S \left[(hk_{0x} \delta + N_{0y}) \frac{\partial^2 W}{\partial y^2} + (hk_{0y} \delta + N_{0x}) \frac{\partial^2 W}{\partial x^2} \right] W dx dy \\ &= \iint_S (hk_{0y} \delta + N_{0x}) \frac{\partial^2 W}{\partial x^2} W dx dy + \iint_S (hk_{0x} \delta + N_{0y}) \frac{\partial^2 W}{\partial y^2} W dx dy \\ &= -\frac{m^2 \pi^2 b (hk_{0y} \delta + N_{0x})}{4a} - \frac{n^2 \pi^2 a (hk_{0x} \delta + N_{0y})}{4b} \\ D &= h \iint_S \left(k_{0x} \frac{\partial^2 \Phi_1}{\partial y^2} + k_{0y} \frac{\partial^2 \Phi_1}{\partial x^2} + \frac{\partial^2 \Phi_2}{\partial y^2} \frac{\partial^2 W}{\partial x^2} + \frac{\partial^2 \Phi_2}{\partial x^2} \frac{\partial^2 W}{\partial y^2} \right) W(x, y) dx dy \\ E &= \iint_S h \left(\frac{\partial^2 \Phi_1}{\partial y^2} \frac{\partial^2 W}{\partial x^2} + \frac{\partial^2 \Phi_1}{\partial x^2} \frac{\partial^2 W}{\partial y^2} \right) W dx dy \\ &= -\frac{hm^2 n^2 \pi^4 (\alpha + \beta)}{2ab} \\ F &= \iint_S \left(\rho V \gamma + \rho \int_0^y \frac{\partial \gamma}{\partial t} d\eta \right) W(x, y) dx dy \end{aligned}$$

It is indispensable to determine $\gamma(x, y, t)$ before solving Eq. (20). According to Biot-Savart law and lifting surface theory (Bisplinghoff *et al.* 1955), the vortex's induced velocity vertical to the membrane surface is

$$v_z(x, y, t) = \frac{1}{4\pi} \int_0^a \int_0^b \frac{\gamma(\xi, \eta, t)}{(x-\xi)^2} \left[1 + \frac{y-\eta}{\sqrt{(x-\xi)^2 + (y-\eta)^2}} \right] d\xi d\eta \quad (21)$$

Combining the boundary condition Eq. (8), an integral equation about $\gamma(x, y, t)$ can be determined as follows

$$\frac{\partial z}{\partial t} + V \frac{\partial z}{\partial x} = \frac{1}{4\pi} \int_0^a \int_0^b \frac{\gamma(\xi, \eta, t)}{(x-\xi)^2} \left[1 + \frac{y-\eta}{\sqrt{(x-\xi)^2 + (y-\eta)^2}} \right] d\xi d\eta \quad (22)$$

Assume the curved surface function of the membrane structure is

$$z(x, y, t) = z_0(x, y) + w(x, y, t) \quad (23)$$

Substituting Eq. (23) into Eq. (22) yields

$$\frac{1}{4\pi} \int_0^a \int_0^b \frac{\gamma(\xi, \eta, t)}{(x-\xi)^2} \left[1 + \frac{y-\eta}{\sqrt{(x-\xi)^2 + (y-\eta)^2}} \right] d\xi d\eta = V \frac{\partial z_0}{\partial y} + V \frac{\partial w}{\partial y} + \frac{\partial w}{\partial t} \quad (24)$$

Substituting Eqs. (1) and (14) into Eq. (24) yields

$$\begin{aligned} & \frac{1}{4\pi} \int_0^a \int_0^b \frac{\gamma(\xi, \eta, t)}{(x-\xi)^2} \left[1 + \frac{y-\eta}{\sqrt{(x-\xi)^2 + (y-\eta)^2}} \right] d\xi d\eta \\ & = V \frac{-8f_1(y-\frac{b}{2})}{b^2} + V \frac{n\pi}{b} \sin \frac{m\pi x}{a} \cos \frac{n\pi y}{b} T(t) + T'(t) \sin \frac{m\pi x}{a} \sin \frac{n\pi y}{b} \end{aligned} \quad (25)$$

According to vortex lattice method (Finnemore *et al.* 2001), the membrane surface is divided into finitely small vortex lattice. In Eq. (25), assume that the vortex density of the j th vortex lattice is

$$\gamma_j = a_{0j} + a_{1j} T(t) + a_{2j} \frac{T'(t)}{V}, \quad (j=1, 2, \dots, M \times N) \quad (26)$$

$$\left. \begin{aligned} \sum_{j=1}^{M \times N} C_{ij} a_{0j} &= -8f_1(y_i - b/2)/b^2, & (i=1,2,\dots,M \times N) \\ \sum_{j=1}^{M \times N} C_{ij} a_{1j} &= \frac{n\pi}{b} \sin \frac{m\pi x_i}{a} \cos \frac{n\pi y_i}{b}, & (i=1,2,\dots,M \times N) \\ \sum_{j=1}^{M \times N} C_{ij} a_{2j} &= \sin \frac{m\pi x_i}{a} \sin \frac{n\pi y_i}{b}, & (i=1,2,\dots,M \times N) \end{aligned} \right\} (27)$$

where a_{0j} , a_{1j} and a_{2j} = constant coefficients obtained from solving linear algebraic equations in vortex lattice method; M, N = the numbers of vortex lattice equally divided in direction x and y , respectively; C_{ij} is a dimensionless geometric sense, and can be obtained by Biot-Savart law.

The vortex density is

$$\gamma = aV\gamma_j = aV \left(a_{0j} + a_{1j}T(t) + a_{2j} \frac{T'(t)}{V} \right), \quad (j=1,2,\dots,M \times N) \quad (28)$$

Substituting Eq. (28) into Eq. (20) yields

$$A_1 T''(t) + B_1 T'(t) - C_1 T(t) - DT^2(t) - ET^3(t) - F_1 = 0 \quad (29)$$

where

$$\begin{aligned} A_1 &= A - \rho a \iint_S \left(\int_0^y a_{2j} d\eta \right) W(x, y) dx dy \\ B_1 &= B - \rho a V \iint_S \left(\int_0^y a_{1j} d\eta \right) W(x, y) dx dy - \rho a V \iint_S a_{2j} W(x, y) dx dy \\ C_1 &= C + \rho a V^2 \iint_S a_{1j} W(x, y) dx dy \\ F_1 &= \rho a V^2 \iint_S a_{0j} W(x, y) dx dy \end{aligned}$$

Obviously, Eq. (29) is a nonlinear differential equation with respect to $T(t)$. Assume that the periodic solution which satisfies the initial condition $T(t)|_{t=0} = 0$ is

$$T(t) = f \sin \omega t = f \sin \theta \quad (30)$$

where f denotes the amplitude.

Substituting Eq. (30) into Eq. (29) and applying the Bubnov-Galerkin method again yields

$$\begin{aligned} & \int_0^{T_0} [A_1 T''(t) + B_1 T'(t) - C_1 T(t) - DT^2(t) - ET^3(t) - F_1] \sin \theta dt \\ &= \int_0^{T_0} (-A_1 f \omega^2 \sin \theta + B_1 f \omega \cos \theta - C_1 f \sin \theta - Df^2 \sin^2 \theta - Ef^3 \sin^3 \theta - F_1) \sin \theta dt \\ &= -f \int_0^{T_0} (A_1 \omega^2 + C_1 + \frac{3}{4} Ef^2) \sin^2 \theta dt + B_1 f \omega \int_0^{T_0} \cos \theta \sin \theta dt - Df^2 \int_0^{T_0} \sin^3 \theta dt \\ &+ \frac{1}{4} Ef^3 \int_0^{T_0} \sin 3\theta \sin \theta dt - F_1 \int_0^{T_0} \sin \theta dt \\ &= 0 \end{aligned} \quad (31)$$

where T_0 is a cycle, $T_0 = 2\pi / \omega$.

Integrating and simplifying Eq. (31) yields

$$-f \int_0^{T_0} (A_1 \omega^2 + C_1 + \frac{3}{4} Ef^2) \sin^2 \theta dt = 0 \quad (32)$$

For $f \neq 0$, and there will be

$$A_1 \omega^2 + C_1 + \frac{3}{4} Ef^2 = 0 \quad (33)$$

When the wind velocity is approaching the critical value, the increasing aerodynamic force will equal or even exceed the sum of dead weight and inertia force of the structure. At that moment, the frequency of the system characteristic equation becomes zero and the divergence instability phenomenon occurs (Kornecki *et al.* 1976).

The critical condition for divergence instability is $\omega = 0$. Substituting A_1, C_1, E and $\omega = 0$ into Eq. (33) yields the critical velocity of divergence instability

$$V_{cr} = \pi \sqrt{\frac{m^2 b (hk_{0y} \delta + N_{0x}) / 4a + n^2 a (hk_{0x} \delta + N_{0y}) / 4b + 3hm^2 n^2 \pi^2 (\alpha + \beta) f^2 / 8ab}{\rho a \alpha_3}} \quad (34)$$

where

$$\begin{aligned} \alpha_3 &= \iint_S a_{1j} W(x, y) dx dy \\ &= \sum_{j=1}^{M \times N} a_{1j} \sin \frac{m\pi x_j}{a} \sin \frac{n\pi y_j}{b} \cdot \frac{a}{M} \cdot \frac{b}{N} \\ &= \frac{ab}{MN} \sum_{j=1}^{M \times N} a_{1j} \sin \frac{m\pi x_j}{a} \sin \frac{n\pi y_j}{b} \end{aligned} \quad (35)$$

From Eq. (33) it can be concluded that in large amplitude theory, the vibration frequency ω is connected to the amplitude f , which is just one of the characteristics of geometrically nonlinear structures.

When f approaches zero, Eq. (34) can be transformed into the formula obtained just according to the small amplitude theory, as follows

$$V_{cr} = \pi \sqrt{\frac{m^2 b (hk_{0y} \delta + N_{0x}) / 4a + n^2 a (hk_{0x} \delta + N_{0y}) / 4b}{\rho a \alpha_3}} \quad (36)$$

In Eq. (34), let $\varepsilon = f_1 / b = 0$. The formula of the planar model can also be obtained in considering the flow separation, as follows

$$V_{cr} = \pi \sqrt{\frac{m^2 b N_{0x} / 4a + n^2 a N_{0y} / 4b + 3hm^2 n^2 \pi^2 (\alpha + \beta) f^2 / 8ab}{\rho a \alpha_3}} \quad (37)$$

4. Computational examples and discussion

As seen in Eq. (34) that the critical velocity of divergence instability V_{cr} is connected to the membrane parameters, structure sizes, prestress, orders and amplitude. For study in this paper, we just take a membrane material commonly applied in projects as an example: $E_1=1400\text{MPa}$; $E_2=900\text{MPa}$; $\rho=1.226 \text{ kg/m}^3$ and $h=0.001\text{m}$. $\lambda = a/b$ = ratio of span across-wind (x) to along-wind (y); $\gamma = N_{0y} / N_{0x}$ = ratio of prestress in y to x ; $\varepsilon = f_1 / b =$

ratio of sag to span in y . The value of α_3 can be obtained by the numerical integration method when all parameters are determine¹. The following parametric analysis will be contrasted with the situation without considering flow separation (Xu *et al.* 2011).

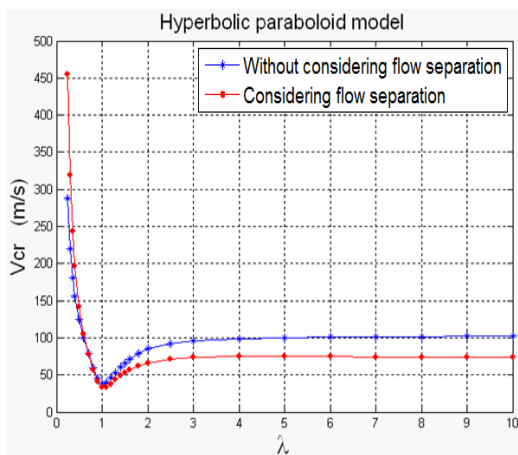
4.1 Span ratio λ

The curve of span ratio and critical wind velocity is shown in Fig. 2 ($b=20$ m; $m=n=1$; $f=1$ m; $N_{0y}=2$ kN/m; $\gamma=1$; $\varepsilon=0.1$). With the increase of span ratio λ , and we compare the two cases: considering or without considering the flow separation.

In Figs. 2(a) and 2(b), the two cases have same change trend with the increase of span ratio λ : when $\lambda \leq 1$, V_{cr} decreases sharply; when $\lambda > 1$, V_{cr} increases gradually; when $\lambda > 3$,

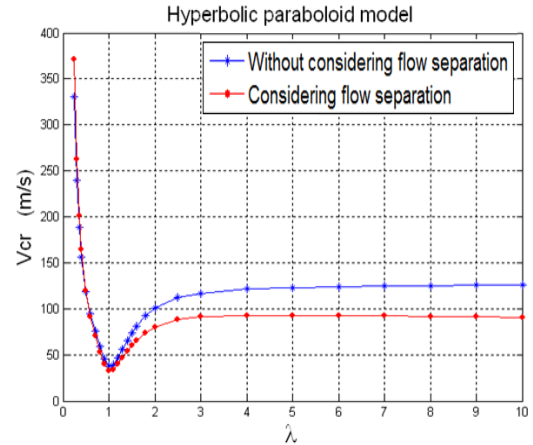
V_{cr} increases gently. It shows that the near-span size ($a \approx b$) should be avoided in hyperbolic paraboloid structures. When $\lambda \leq 0.7$, the V_{cr} in considering flow separation is greater than the situation without considering it, and the smaller the λ , the greater the D-value. But it is just opposite when $\lambda \geq 0.7$, a greater V_{cr} we will get without considering flow separation, the greater the λ , the greater the D-value, and when $\lambda > 3$, D-value remains basically invariable.

For the orthotropy of membrane, Fig. 2(c) shows that without considering flow separation, a greater V_{cr} can be obtained if the smaller modulus is arranged in the along-wind direction when $\lambda \neq 1$ (just as $E_2 < E_1$), the more discrepant the two span sizes (b and a), the greater the D-value. When $\lambda=1$, the two V_{cr} values are equal.

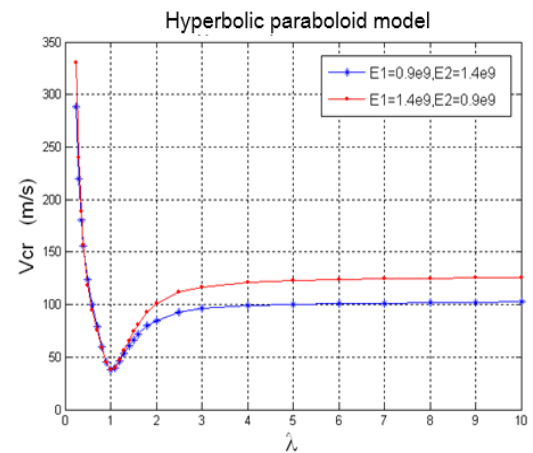


(a) $E_2=1400\text{MPa}$, $E_1=900\text{MPa}$

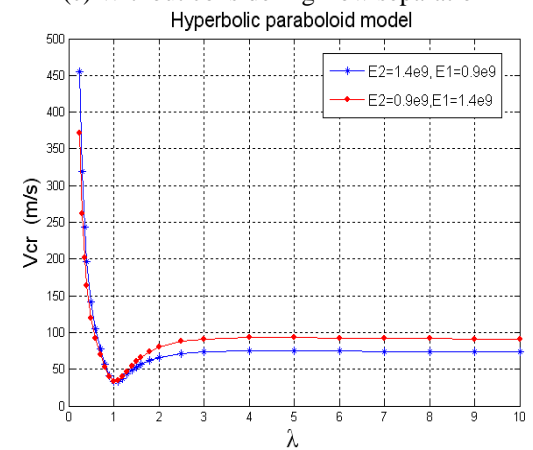
Continued-



(b) $E_2=900\text{MPa}$, $E_1=1400\text{MPa}$



(c) Without considering flow separation



(d) Considering flow separation

Fig. 2 Curve of a -to- b ratio λ and critical wind velocity V_{cr}

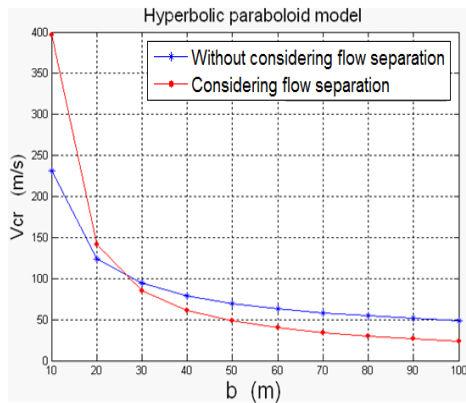
In Fig. 2(d), when consider flow separation, it is consistent with the case without considering it when $\lambda \geq 1$, but when $\lambda < 1$, the larger modulus should be arranged in the along-wind direction (just as $E_1 < E_2$) to get a greater V_{cr} .

¹ Please contact the author to get the computing program as necessary.

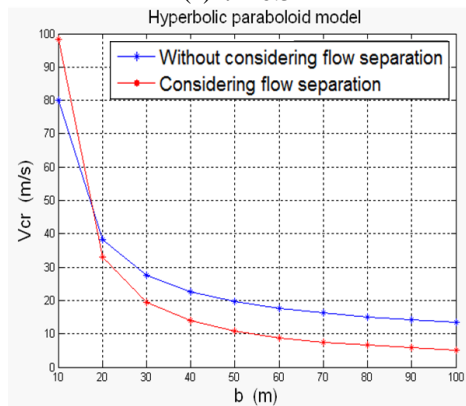
4.2 Along-wind span b

The curve of along-wind span and critical wind velocity is shown in Fig. 3. ($m=n=1; f=1\text{ m}, N_{0y}=2\text{ kN/m}; \gamma=1; \varepsilon=0.1$)

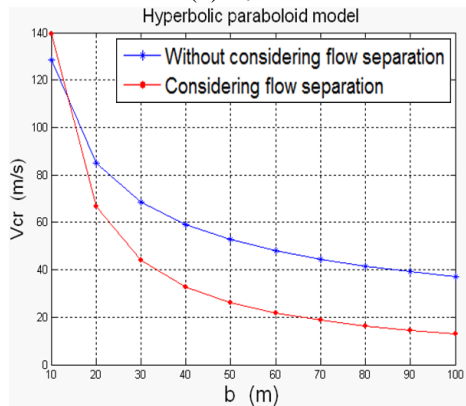
At different λ , with the increase of span b , V_{cr} decreases gradually both in the two situations of considering flow separation or without it. When $b \leq 30\text{ m}$, it decreases sharply; when $b > 30\text{ m}$, it decreases gently. When b is small, V_{cr} in considering flow separation is greater than the situation without considering it.



(a) $\lambda = 0.5$



(b) $\lambda = 1$



(c). $\lambda = 2$

Fig. 3 Curve of span b and critical wind velocity V_{cr}

But with b increasing, V_{cr} in considering flow separation becomes smaller than the situation without considering it. V_{cr} of the two situations are equal when b reaches a certain value, and the greater the λ , the smaller the certain span b .

4.3 Prestress N_{0y}

The curve of prestress N_{0y} and critical wind velocity is shown in Fig. 4. ($m=n=1; f=1\text{ m}; b=20\text{ m}; \gamma=1; \varepsilon=0.1$)

At different λ , with the increase of N_{0y} , V_{cr} increases gradually, and it present approximate linearization in general. This is consistent with the situation without considering flow separation. The D-value of the two situations remains basically invariable with the increase of N_{0y} .

4.4 Ratio of N_{0y} -to- N_{0x} γ

The curve of the N_{0y} -to- N_{0x} ratio γ and critical wind velocity is shown in Fig. 5. ($m=n=1; f=1\text{ m}, b=20\text{ m}; N_{0y}=2\text{ kN/m}; \varepsilon=0.1$)

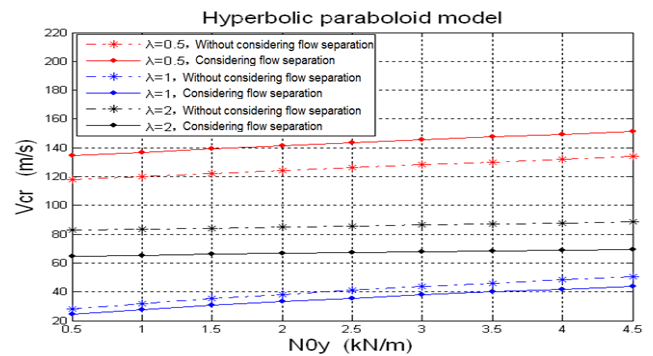


Fig. 4 Curve of pretension N_{0y} and critical wind velocity V_{cr}

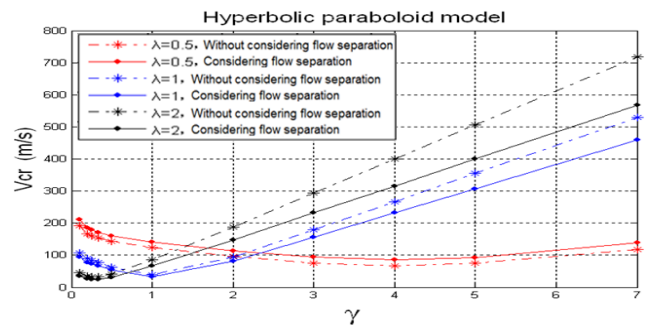


Fig. 5 Curve of N_{0y} -to- N_{0x} ratio γ and critical wind velocity V_{cr}

At different λ , with the increase of γ , V_{cr} presents a descending branch (the smaller the λ , the longer the branch) at first then increases gradually (the larger λ is, the more sharply it increases). This is consistent with the situation without considering flow separation. The D-value of the two situations increases with the increase of γ too.

4.5 Sag-to-span ratio ε

The curve of the ratio of sag-to-span and critical wind velocity is shown in Fig. 6 ($m=n=1$; $b=20$ m; $f=1$ m; $N_{0y}=2$ kN/m).

At different λ , V_{cr} increases gradually with the increase of ε both in considering flow separation or without considering it. The D-value of the two situations increases with the increase of ε too. But when f_1 and f_2 are close to each other (e.g., $f_1=f_2$ when $\gamma=1, \lambda=1$ or $\gamma=0.25, \lambda=2$), the increasing ε has little effect on the structural stability.

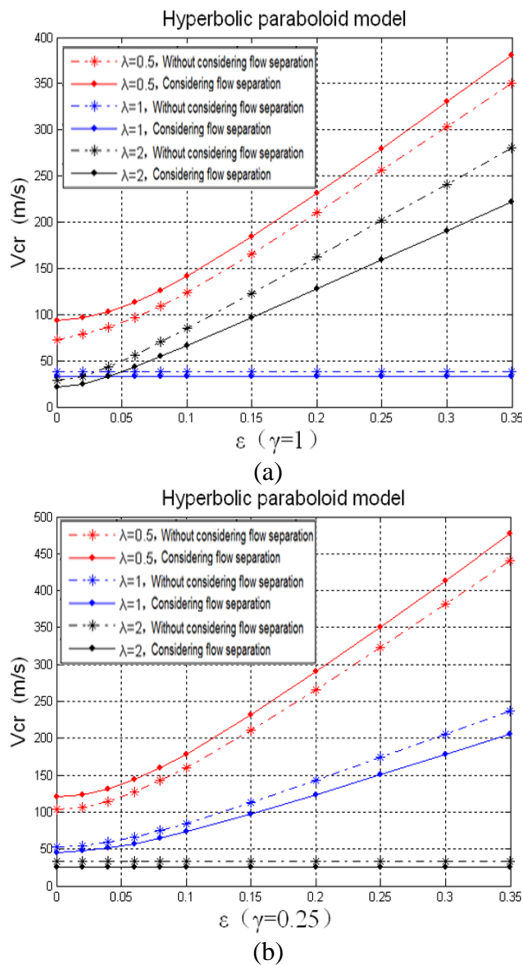


Fig. 6 Curve of the ratio of sag-to-span ε and critical wind velocity V_{cr}

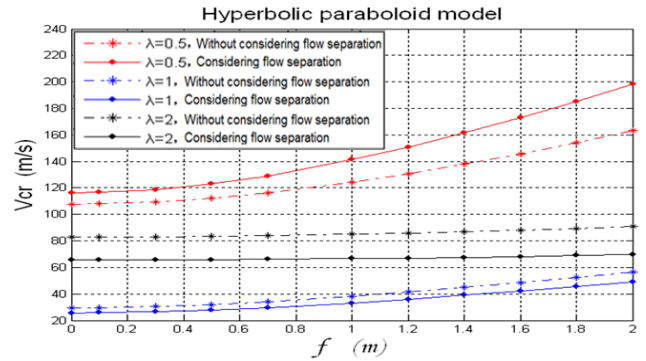


Fig. 7 Curve of amplitude f and critical wind velocity

4.6 Amplitude f

The curve of amplitude and critical wind velocity is shown in Fig. 6 ($m=n=1$; $\gamma=1$; $b=20$ m; $N_{0y}=2$ kN/m; $\varepsilon=0.1$).

At different λ , V_{cr} increases gradually with the increase of amplitude f both in considering flow separation or without considering it. The D-value of the two situations increases with the increase of f too.

4.7 Orders m, n

The critical wind velocities with different orders are shown in Table 1 ($\gamma=1$; $f=1$ m; $b=20$ m; $N_{0y}=2$ kN/m; $\varepsilon=0.1$; values in brackets are the results without considering flow separation).

At different orders, the trend of divergence instability has a big difference in considering flow separation or without considering it. Without considering flow separation, the trend of divergence instability in sag direction is same as the situation in arch direction (Xu *et al.* 2011): when $\lambda < 1$, the trend of divergence instability presents a high order along the wind direction ($n > m=1$), the smaller λ is, the higher the order (n) will be; when $\lambda > 1$, it's just the opposite: it presents a high order across the wind direction ($m > n=1$), the larger λ is, the higher the order (m) will be; when $\lambda=1$, it presents a low order instability ($n=m=1$). In considering flow separation, the model presents low order instability ($m=n=1$) when $\lambda \leq 1$ and high order instability along the wind direction ($n=3, m=1$) when $\lambda > 1$.

5 Conclusions

Considering the influence of flow separation and geometric nonlinearity, an analytical method was used to study the aerodynamic stability of hyperbolic paraboloid orthotropic membrane structure in the large amplitude theory, and the critical velocity of divergence instability formula was obtained. Comparing with the model without considering flow separation, the main analysis results are summarized as follows:

Table 1 Critical wind velocity V_{cr} with different orders (m/s)

Order	$n=m=1$	$n=2,m=1$	$n=3,m=1$	$n=1,m=2$	$n=1,m=3$	$n=m=2$	$n=m=3$
$\lambda=0.25$	454.61 (288.18)	864.93 (191.56)	1319.9 (164.18)	727.14 (1233.63)	1033.6 (2190.62)	1202.58 (861.61)	2203.79 (1655.66)
$\lambda=0.5$	141.25 (124.04)	182.87 (71.26)	307.55 (98.96)	261.8 (352.05)	415.27 (785.36)	250.25 (216.38)	432.62 (371.61)
$\lambda=1$	33.13 (38.21)	66.02 (73.74)	87.61 (97.9)	139.41 (148.05)	250.31 (261.02)	68.64 (75.06)	115.41 (125.63)
$\lambda=2$	66.57 (85.95)	60.78 (80.54)	54.86 (99.03)	60.19 (39.59)	157.09 (98.21)	61.93 (74.86)	78.43 (99.96)
$\lambda=4$	75.12 (98.92)	62.41 (81.72)	51.79 (99.3)	81.67 (84.28)	122.34 (55.89)	67.08 (80.63)	76.67 (99.47)

- Same with the model without considering flow separation, it is of positive significance to arrange the membrane's warp and weft rationally according the local wind regime to prevent a destructive instability of the structure. Additionally, the stress increment, which is acquired under geometric nonlinearity, can improve the lateral rigidity and enhance the aerodynamic stability of structure. The two results tally more with the actual situation. And with an initial force (which can be obtained by the local basic wind pressure) acting on the membrane, a reference value of amplitude can be determined.

- Same with the model without considering flow separation, the analysis and comparison of various preceding parameters in considering it shows that, the span ratio λ plays a more complex role than the others in the aerodynamic stability of membrane structures, so as the main control parameter in designing this kind of structure, it needs to be given sufficient attention.

- There is a little inconsistency about the aerodynamic stability regularities between the two models (in considering or without considering the flow separation). And the critical wind velocities obtained from in the two situations have significant difference. Obviously, considering flow separation is more tally with the actual. So in studying aerodynamic stability of a membrane structure with sharp corner in leading edge (just like the hyperbolic paraboloid membrane structure in its sag direction), the influence of flow separation can't be neglected.

The critical wind-velocity formula obtained in this paper has provided a reference for the aerodynamic stability of the membrane structure in flow separation. The discussions above show that the damping coefficient ζ_0 has no effect on the aerodynamic stability of structures. Therefore, numerical analysis and experimental studies will be presented based on the results given in this paper in subsequent work.

Acknowledgments

This work is supported by the National Natural Science Foundation of China, China (Project Number: 51608060).

References

- Attar, P.J. and Dowell, E.H. (2005), "A reduced order system ID approach to the modelling of nonlinear structural behavior in aeroelasticity", *J. Fluid. Struct.*, **21**(5-7), 531-542.
- Awrejcewicz, J. (2013), "Large amplitude free vibration of orthotropic shallow shells of complex shapes with variable thickness", *Latin American J. Solids Struct.*, **10**(10), 149-162.
- Banichuk, N., Jeronen, J., Neittaanmaki, P. and Tuovinen, T. (2010a), "Static instability analysis for travelling membranes and plates interacting with axially moving ideal fluid", *J. Fluid. Struct.*, **26**(2), 274-291.
- Banichuk, N., Jeronen, J., Neittaanmaki, P. and Tuovinen, T. (2010b), "On the instability of an axially moving elastic plate", *Int. J. Solids Struct.*, **47**(1), 91-99.
- Bisplinghoff, R.L., Ashley, H. and Halfman, R.L. (1955), *Aeroelasticity*, Addison-Wesley, New Jersey, America.
- Dowell, E.H. (1970), "Panel flutter: A review of the aeroelastic stability of panel and shells", *AIAA J.*, **8**(3), 385-399.
- Finnemore, E.J. and Franzini, J.B. (2001), *Fluid Mechanics with Engineering Applications*, McGraw-Hill Companies, New York, America.
- Forsching, H.W. (1982), *Principles of aeroelasticity*, Shanghai Science and Technology Literature Press, Shanghai, China (in Chinese).
- Ivovich, V.A. and Pokrovskii, L.N. (1991), *Dynamic analysis of suspended roof systems*, A.A. Balkema, Rotterdam, Netherlands.
- Kawakita, S., Bienkiewicz, B. and Cermak, J.E. (1992), "Aeroelastic model study of suspended cable roof", *J. Wind Eng. Ind. Aerod.*, **42**, 1459-1470.
- Kornecki, A., Dowell, E.H. and O'Brien, J. (1976), "On the aeroelastic instability of two-dimensional panels in uniform incompressible flow", *J. Sound Vib.*, **47**(2), 163-178.
- Li, Q.X. and Sun, B.N. (2006), "Wind-induced aerodynamic instability analysis of the closed membrane roofs", *J. Vib. Eng.*, **19**(3), 346-353 (in Chinese).
- Liu, C.J., Zheng, Z.L., Long, J., Guo, J.J. and Wu, K. (2013), "Dynamic analysis for nonlinear vibration of prestressed orthotropic membranes with viscous damping", *Int. J. Struct. Stab. Dynam.*, **13**(2), 60-66.
- Liu, M., Chen, X. and Yang, Q. (2016), "Characteristics of dynamic pressures on a saddle type roof in various boundary layer flows", *J. Wind Eng. Ind. Aerod.*, **150**, 1-14.
- Minami, H. (1998), "Added mass of a membrane vibrating at finite amplitude", *J. Fluid. Struct.*, 1998, **12**, 919-932.
- Minami, H., Okuda, Y. and Kawamura, S. (1993), "Experimental studies on the flutter behavior of membranes in a wind tunnel." *Space Structures 4*, (Eds., G.A.R. Parke and C.M. Howard) Vol.1, Thomas Telford, London.
- Miyake, A., Yoshimura, T. and Makino, M. (1992), "Aerodynamic instability of suspended roof modals", *J. Wind Eng. Ind. Aerod.*,

- 42, 1471-1482.
- Munteanu, S.L., Rajadas, J., Nam, C. and Chattopadhyay, A. (2015), "Reduced-order-model approach for aeroelastic analysis involving aerodynamic and structural nonlinearities", *AIAA J.*, **43**(3), 560-571.
- Rizzo, F. and Ricciardelli, F. (2016), "Design approach of wind load for Hyperbolic paraboloid roof with circular and elliptical plan", *Eng. Struct.*, **139**, 153-169.
- Rizzo, F. and Sepe, V. (2015), "Static loads to simulate dynamic effects of wind on hyperbolic paraboloid roofs with square plan", *J. Wind Eng. Ind. Aerod.*, **137**, 46-57.
- Scott, R.C., Bartels, R.E. and Kandil, O.A. (2007), "An aeroelastic analysis of a thin flexible membrane", *Propulsion Conferences, 48th AIAA/ASME/ASCE/AHS/ASC Structures, Structural Dynamics and Materials Conference*, American Institute of Aeronautics and Astronautics (AIAA), Reston, VA.
- Shin, C.J., Kim, W. and Chung, J.T. (2004), "Free in-plane vibration of an axially moving membrane", *J. Sound Vib.*, **272**(1-2), 137-154.
- Stanford, B. and Ifju, P. (2008), "Fixed membrane wings for micro air vehicles: Experimental characterization, numerical modeling, and tailoring", *Prog. Aerosp. Sci.*, **44**(4), 258-294.
- Stanford, B. and Sytsma, M. (2007), "Static aeroelastic model validation of membrane micro air vehicle wings", *AIAA J.*, **45**(12), 2828-2837.
- Sun, B.N., Mao, G.D. and Lou, W.J. (2003), "Wind induced coupling dynamic response of closed membrane structures", *Proceedings of the 11th Int. Conf. On Wind Engineering, International Association for Wind Engineering*, Atsugi, Japan.
- Sygulski, R. (1994), "Dynamic analysis of open membrane structures interaction with air", *Int. J. Numer. Meth. Eng.*, **37**(11), 1807-1823.
- Sygulski, R. (1997), "Numerical analysis of membrane stability in air flow", *J. Sound Vib.*, **201**(3), 281-292.
- Tang, D.M. and Dowell, E.H. (2015), "Experimental and theoretical study for nonlinear aeroelastic behavior of a flexible rotor blade", *AIAA J.*, **31**(31), 1133-1142.
- Uematsu, Y., Arakatsu, F. and Matsumoto, S. (2009), "Wind force coefficients for designing hyperbolic paraboloid free-roofs", *Nctam Papers, National Congress of Theoretical & Applied Mechanics*, Japan, **58**, 175-175.
- Vassilopoulou, I. and Gantes, C.J. (2012), "Nonlinear dynamic phenomena in a SDOF model of cable net", *Arch. Appl. Mech.*, **82**(10-11), 1689-1703.
- Xu, X.P., Zheng, Z.L., Liu, C.J., Song, W.J. and Long, J. (2011), "Aerodynamic stability analysis of geometrically nonlinear orthotropic membrane structure with hyperbolic paraboloid", *J. Eng. Mech.*, **137**(11), 759-768.
- Yang, Q. and Liu, R. (2005), "On aerodynamic stability of membrane structures", *Int. J. Space Struct.*, **20**(3), 181-188.
- Yang, Q.S. and Liu, R.X. (2006), "Studies on aerodynamic stability of membrane structures", *Eng. Mech.*, **23**(9), 18-24(in Chinese).
- Yang, Q., Wu, Y. and Zhu, W. (2010), "Experimental study on interaction between membrane structures and wind environment", *Earthq. Eng. Eng. Vib.*, **9**(4), 2010.
- Zheng, Z.L., Xu, X.P., Liu, C.J., Song, W.J. and Long, J. (2010), "Nonlinear aerodynamic stability analysis of orthotropic membrane structures with large amplitude", *Struct. Eng. Mech.*, **37**(4), 401-413.

Appendix I

The critical velocity is

$$V = \pi \sqrt{\frac{m^2 b (hk_{0y} \delta + N_{0x}) / 4a + n^2 a (hk_{0x} \delta + N_{0y}) / 4b + 3hm^2 n^2 \pi^2 (\alpha + \beta) f^2 / 8ab}{\rho a \alpha_3}}$$

where

$$\alpha = \frac{E_2 a^2 n^2}{32 b^2 m^2}, \quad \beta = \frac{E_1 b^2 m^2}{32 a^2 n^2}, \quad \delta = \frac{k_{0x} (n\pi/b)^2 + k_{0y} (m\pi/a)^2}{(n\pi/b)^4 / E_1 + (m\pi/a)^4 / E_2}$$

$$\begin{aligned} \alpha_3 &= \iint_S a_{1j} W(x, y) dx dy \\ &= \sum_{j=1}^{M \times N} a_{1j} \sin \frac{m\pi x_j}{a} \sin \frac{n\pi y_j}{b} \cdot \frac{a}{M} \cdot \frac{b}{N} \\ &= \frac{ab}{MN} \sum_{j=1}^{M \times N} a_{1j} \sin \frac{m\pi x_j}{a} \sin \frac{n\pi y_j}{b} \end{aligned}$$

$$\lambda = a/b, \quad \gamma = N_{0y} / N_{0x}, \quad \varepsilon = f_1 / b.$$

For study, we just take a membrane material commonly applied in projects as an example: $E_1=1400\text{MPa}$; $E_2=900\text{MPa}$; $\rho=1.226 \text{ kg/m}^3$; $h=0.001 \text{ m}$; $b=20 \text{ m}$; $m=n=1$; $f=1 \text{ m}$; $N_{0y}=2 \text{ kN/m}$; $\gamma=1$ and $\varepsilon=0.1$. Take λ as a variable.

By FORTRAN Program, the numerical calculation procedure is as follows

```
PROGRAM MAIN
IMPLICIT NONE
REAL,PARAMETER::PP=1.226,PI=3.1415926,E2=1.
4E9,E1=0.9E9,H=0.001
INTEGER,PARAMETER::M=33,N=33,Q=M*N      !
Divided into 33 equal parts.
DIMENSION
A(Q,Q),B(Q),X0(Q),X1(Q),X2(Q),Y0(Q),Y1(Q),Y2(Q),
X(Q),JS(Q)
REAL
A,B,X0,X1,X2,Y0,Y1,Y2,S,V,X,A3,AA,BB,VV1(35),R,E,
F0,A1,B1,NOX,
&      NOY,VCR,F1,F2,KOX,KOY,TT
INTEGER KK,LL,II,L1,L2,I,J,L,JS
DATAVV1/0.1,0.11,0.12,0.13,0.14,0.16,0.18,0.2,0.25,0.
```

3,0.35,0.4,0.5,0.6,0.7,

&

0.8,0.9,1,1.1,1.2,1.3,1.4,1.5,1.6,1.8,2,2.5,3,4,5,6,7,8,9,10/

NOY=2000.0

E=0.1

F0=1

KK=1

LL=1

R=1

BB=20

DO II=1,35

V=VVI(II)

AA=BB*V

NOX=NOY/R

F1=BB*E

F2=F1*R*V**2

KOX=8*F2/AA**2

KOY=-8*F1/BB**2

A1=E2*LL**2/(32*V**2*KK**2)

B1=E1*KK**2*V**2/(32*LL**2)

TT=(KOX*(LL*PI/BB)**2+KOY*(KK*PI/AA)**2)/(
(LL*PI/BB)**4/E1+(KK*

&

PI/AA)**4/E2)

DO L2=1,N

DO L1=1,M

I=(L1-1)*N+L2

X0(I)=AA/M*(L1-0.5)

```

        Y0(I)=BB/N*(L2-0.25)
    END DO
END DO
DO L2=1,N
    DO L1=1,M
        J=(L1-1)*N+L2
        X1(J)=AA/M*(L1-1.0)
        Y1(J)=BB/N*(L2-0.75)
        X2(J)=AA/M*L1
        Y2(J)=BB/N*(L2-0.75)
    END DO
END DO
DO I=1,Q
    DO J=1,Q
        A(I,J)=AA/(4*PI)*(1.0/((Y0(I)-Y1(J))*(X0(I)-
            X2(J))-(Y0(I)-Y2(J))*(X0(I)-
&
            -X1(J))))*((Y2(J)-Y1(J))*(Y0(I)-
Y1(J))+(X2(J)-X1(J))*(X0(I)
&
            -X1(J)))/SQRT(((Y0(I)-
Y1(J))**2+(X0(I)-X1(J))**2)-((Y2(J)-Y1(J)
&
            *(Y0(I)-Y2(J))+(X2(J)-X1(J))*(X0(I)-
X2(J)))/SQRT((Y0(I)-Y2(J)
&
            **2+(X0(I)-X2(J))**2))+1.0/(X1(J)-
X0(I))*(1.0+(Y0(I)-Y1(J))/
&
            SQRT((Y0(I)-Y1(J))**2+(X0(I)-
X1(J))**2))-1.0/(X2(J)-X0(I))*
&
            (1.0+(Y0(I)-Y2(J))/SQRT((Y0(I)-
Y2(J))**2+(X0(I)-X2(J))**2)))
    END DO
END DO
DO I=1,Q
    B(I)=LL*PI/BB*SIN(KK*PI*X0(I)/AA)*COS(LL
*PI*Y0(I)/BB)
END DO
A3=0
        CALL AGAUS(A,B,Q,X,L,JS)
    IF(L.NE.0) THEN
        DO I=1,Q
            S=AA*BB/(M*N)*X(I)*SIN(KK*PI*X0(I)/AA)
            *SIN(LL*PI*Y0(I)/BB)
            A3=A3+S
        END DO
    END IF
    VCR=PI*SQRT((KK**2*BB*(NOX+H*TT*K0Y)/(4
        *AA)+LL**2*AA*(NOY
&
        +H*TT*K0X)/(4*BB)+3*H*(KK*LL*PI*F0)**2*(A1+B1)
/
&
        (8*AA*BB)))/(PP*AA*A3))
    WRITE(*,*) "VCR=",VCR
END DO
END
SUBROUTINE AGAUS(A,B,Q,X,L,JS)
INTEGER K,Q,L,JS,IS
DIMENSION A(Q,Q),X(Q),B(Q),JS(Q)
REAL A,B,X,T,D
L=1
DO K=1,Q-1
    D=0.0

```

```

DO I=K,Q           A(K,J)=A(K,J)/A(K,K)
DO J=K,Q           END DO
  IF (ABS(A(I,J)).GT.D) THEN
    B(K)=B(K)/A(K,K)
    D=ABS(A(I,J))
    DO I=K+1,Q
      JS(K)=J
      DO J=K+1,Q
        IS=I
        A(I,J)=A(I,J)-A(I,K)*A(K,J)
      END DO
      B(I)=B(I)-A(I,K)*B(K)
    END DO
  END DO
END DO
IF (D+1.0.EQ.1.0) THEN
  L=0
ELSE
  IF (JS(K).NE.K) THEN
    DO I=1,Q
      T=A(I,K)
      A(I,K)=A(I,JS(K))
      A(I,JS(K))=T
    END DO
  END IF
  IF (IS.NE.K) THEN
    DO J=K,Q
      T=A(K,J)
      A(K,J)=A(IS,J)
      A(IS,J)=T
    END DO
    T=B(K)
    B(K)=B(IS)
    B(IS)=T
  END IF
END IF
IF (L.EQ.0) THEN
  WRITE(*,100)
  RETURN
END IF
DO J=K+1,Q

```

```

A(K,J)=A(K,J)/A(K,K)
END DO
B(K)=B(K)/A(K,K)
DO I=K+1,Q
  DO J=K+1,Q
    A(I,J)=A(I,J)-A(I,K)*A(K,J)
  END DO
  B(I)=B(I)-A(I,K)*B(K)
END DO
END DO
IF (ABS(A(Q,Q))+1.0.EQ.1.0) THEN
  L=0
  WRITE(*,*) "FAIL"
  RETURN
END IF
X(Q)=B(Q)/A(Q,Q)
DO I=Q-1,1,-1
  T=0.0
  DO J=I+1,Q
    T=T+A(I,J)*X(J)
  END DO
  X(I)=B(I)-T
END DO
JS(Q)=Q
DO K=Q,1,-1
  IF (JS(K).NE.K) THEN
    T=X(K)
    X(K)=X(JS(K))
    X(JS(K))=T
  END IF
END DO
RETURN
END

```